Impact of dephasing on nonequilibrium steady-state transport in fermionic chains with long-range hopping

Subhajit Sarkar ⬥,[1,2,*] Bijay Kumar Agarwalla,[3,†] and Devendra Singh Bhakuni[4,5,‡]

[1]*Institute of Theoretical Physics, Jagiellonian University, Łojasiewicza 11, 30-348 Kraków, Poland*

[2]*Department of Physics and Nanotechnology, SRM Institute of Science and Technology, Kattankulathur-603 203, India*

[3]*Department of Physics, Indian Institute of Science Education and Research Pune, Dr. Homi Bhabha Road, Ward No. 8, NCL Colony, Pashan, Pune, Maharashtra 411008, India*

[4]*The Abdus Salam International Centre for Theoretical Physics, Strada Costiera 11, 34151 Trieste, Italy*

[5]*Department of Physics, Ben-Gurion University of the Negev, Beer Sheva 84105, Israel*

Quantum transport in nonequilibrium settings plays a fundamental role in understanding the properties of systems ranging from quantum devices to biological systems. Dephasing—a key aspect of out-of-equilibrium systems—arises from interactions with a noisy environment and can profoundly modify transport properties. Here we investigate the impact of dephasing on the nonequilibrium steady-state transport properties of noninteracting fermions on a one-dimensional lattice with long-range hopping (proportional to $1/r^\alpha$), where $\alpha > 1$. We demonstrate the emergence of distinct transport regimes as the long-range hopping parameter, α, is tuned. In the short-range limit ($\alpha \gg 1$), transport is diffusive. Conversely, in the long-range limit [$\alpha \sim \mathcal{O}(1)$], we observe a superdiffusive transport regime. Using numerical simulations of the Lindblad master equation and corroborating these with an analysis of the current-operator norm, we identify a critical long-range hopping parameter, $\alpha_c \approx 1.5$, below which superdiffusive transport becomes pronounced and rapidly becomes independent of the dephasing strength. Our results elucidate the intricate balance between dephasing and unitary dynamics, revealing steady-state transport features.

I. INTRODUCTION

Quantum transport of charge and energy in nonequilibrium settings is foundational in modern physics, relevant to processes like light harvesting in photosynthesis, chemical reactions in chemical and biological systems [1,2], and emerging nonequilibrium states in nanofabricated quantum devices [3–6]. Specifically, charge transport measurements using quantum dot arrays have led to breakthroughs in Coulomb blockade, Kondo physics, superconductivity, quantum-point-contact universal conductance, and quantum computing [4,7–10].

The study of quantum transport often involves analyzing the temporal behavior of a wave packet's mean squared displacement, or the flow of energy and charge through a system using a boundary drive [11–17]. Ballistic transport results in quadratic growth of the mean squared displacement, while diffusive systems exhibit linear growth of the same in time. Similarly, in boundary-driven setups, a linearly decreasing steady-state current with the system size indicates a diffusive transport, while for a ballistic transport, the steady-state current is independent of the system size. Any deviations from these scaling behaviors signify anomalous transport [18–21].

Dephasing, introduced via environmental coupling, significantly affects quantum transport in lattice systems [15–17,22,23]. This includes Zeno-type dephasing with classical noise, leading to environment-assisted quantum transport [1,24–27]. Dephasing can also result in anomalous transport in localized systems, exhibiting subdiffusive, diffusive, or logarithmic behavior depending on noise sparsity [22,23,28]. Recent research on a boundary-driven system in the nearest-neighbor chain of free fermions suggests a transition from ballistic to diffusive transport with varying dephasing strength [29,30].

Short-range hopping systems have been the main focus in recent times, leaving open questions regarding transport properties in long-range systems with power-law hopping in the presence of dephasing [31–35]. These systems, found in nature and engineered in cold-atom and trapped ionic setups, exhibit significant qualitative changes in various physical properties, including equilibrium phase, ground state, and dynamics [36–46]. For $\alpha \gg d$ (where α is the long-range hopping exponent, and d is the dimension of the system), the physics largely resembles short-range systems, but as α is decreased new universality classes can emerge, new phases can be stabilized [47], and, in the extreme limit but for $\alpha < d$, it introduces novel features like logarithmic entanglement growth, heating suppression, light-cone evolution, and self-trapping [48–53].

Here we investigate the nonequilibrium steady-state (NESS) transport properties of long-range systems coupled

*sbhjt72@gmail.com; subhajis@srmist.edu.in

†bijay@iiserpune.ac.in

‡devendra@post.bgu.ac.il
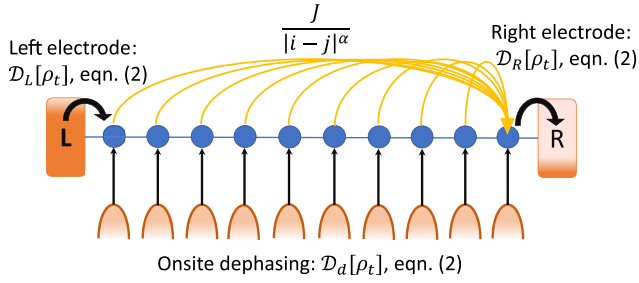
FIG. 1. Schematic of our setup: a noninteracting fermionic lattice chain with long-range hopping (indicated by yellow solid lines) is placed between two baths (electrodes kept at the infinite bias limit: L, left; R, right) injecting and extracting particles at the first and last sites, respectively. At each site of the chain, an on-site dephasing is applied that mimics the Zeno-type measurement of number density at that site, indicated by arrows.

to dissipative particle injection-extraction baths with a rate Γ corresponding to an infinite bias condition and a dephasing environment with a rate γ, using the Lindblad master equation [54,55]. Previous work focused on these systems without dephasing, and subdiffusive conductance scaling was observed under proper tuning of chemical potential bias [56]. A finite bias window also leads to significant non-Markovianity [57,58], which requires further investigation.

Remarkably we observe that above a critical value of the long-range parameter, $\alpha_c \approx 1.5$, the NESS charge current exhibits diffusive scaling with the system size ($J_\infty \sim L^{-1}$). However, below the critical parameter α_c, we observe superdiffusive transport with a power-law dependence on system size for $1 < \alpha < 1.5$, and for $\alpha \leqslant 1$, an inverse logarithmic dependence of current on system size, indicating anomalous transport. These distinctive transport regimes arise due to the interplay between long-range hopping and dephasing, as discussed in subsequent sections. Furthermore, we highlight similarities between the NESS current heat map in the α-γ plane and the entanglement phase diagram of the measurement-induced phase transition (MIPT) in long-range hopping systems [59–61].

II. MODEL HAMILTONIAN AND FORMULATION

We consider a linear chain of L sites hosting noninteracting spinless fermions with long-range hoping, as shown in Fig. 1. The model Hamiltonian for the chain is given by

$$\hat{\mathcal{H}} = \sum_{j=1}^{L-1} \left[\sum_r \frac{J}{r^\alpha} (\hat{c}_j^\dagger \hat{c}_{j+r} + \text{H.c.}) \right] = \sum_{i,j=1}^{L-1} \sum_r \hat{c}_i^\dagger \mathbb{H}_{i,j}^{(r)} \hat{c}_j$$

with $\mathbb{H}_{i,j}^{(r)} = \frac{J}{r^\alpha}(\delta_{i,j+r} + \delta_{i+r,j})$, (1)

where $\frac{J}{r^\alpha}$ is the long-range hopping strength with the exponent of the spatial dependence α, $r = |i - j|$ being the distance between lattice sites i and j. The operator norm of the long-range hopping term is given by $L^{1-\alpha}$, and for $\alpha < 1$, it becomes dominant in the thermodynamic limit [62]. However, one can rescale such a term by an α-dependent factor $\mathcal{N}_\alpha$ which is $\mathcal{N}_\infty = 2$ and $\mathcal{N}_0 = L$ [63–66]. Nevertheless, since experiments are performed with a finite number of sites, such

rescaling does not appear naturally [3,31,32,67]. Therefore, we do not consider this rescaling in our paper. We couple the system to a particle injecting source and a particle extraction sink to the left and right end, respectively, with a constant rate Γ. Additionally, we add Zeno-type dephasing at each site with strength γ providing an energy relaxation channel. The equation of motion of the density matrix of the system is governed by the standard Lindblad quantum master equation:

$$\frac{\partial \rho_t}{\partial t} = -i[\hat{\mathcal{H}}, \rho_t] + \mathcal{D}_d[\rho_t] + \mathcal{D}_L[\rho_t] + \mathcal{D}_R[\rho_t],$$

$$\mathcal{D}_d[\rho_t] = \frac{\gamma}{2} \sum_{j=1}^{L} \left(\hat{n}_j \rho_t \hat{n}_j - \frac{1}{2}\{\hat{n}_j, \rho_t\} \right),$$

$$\mathcal{D}_L[\rho_t] = \frac{\Gamma}{2} \left(\hat{c}_1^\dagger \rho_t \hat{c}_1 - \frac{1}{2}\{\hat{c}_1 \hat{c}_1^\dagger, \rho_t\} \right),$$

$$\mathcal{D}_R[\rho_t] = \frac{\Gamma}{2} \left(\hat{c}_L \rho_t \hat{c}_L^\dagger - \frac{1}{2}\{\hat{c}_L^\dagger \hat{c}_L, \rho_t\} \right),$$ (2)

where $\mathcal{D}_d[\rho_t]$, $\mathcal{D}_L[\rho_t]$, and $\mathcal{D}_R[\rho_t]$ are the Lindblad dissipators corresponding to the on-site dephasing, left, and right boundary drive, respectively, and $\hat{n}_i$ is the fermion number operator at site i.

For the long-range Hamiltonian, the local current is defined from the particle number conservation [27]: $\frac{d\hat{n}_j}{dt} = \hat{J}_{j,\text{in}} - \hat{J}_{j,\text{out}}$. For the site connected to the left lead, the current into the first site is $\hat{J}_{1,\text{in}} = \mathcal{D}_L[\hat{n}_1] = \Gamma(1 - \hat{n}_1)$ and the current out of the first site is $\hat{J}_{1,\text{out}} = i[\hat{\mathcal{H}}, \hat{n}_1]$. Similarly, for the last site connected to the right lead, the current into the last site is $\hat{J}_{L,\text{in}} = i[\hat{\mathcal{H}}, \hat{n}_L]$ and the current out of the last site is $\hat{J}_{L,\text{out}} = \mathcal{D}_R[\hat{n}_L] = \Gamma\hat{n}_L$. For all other sites, i.e., $2 \leqslant j \leqslant L - 1$, $\hat{J}_{j,\text{in}} - \hat{J}_{j,\text{out}} = i[\hat{\mathcal{H}}, \hat{n}_j]$, which gives

$$\hat{J}_{j,\text{in}} = -i \sum_r \frac{J}{r^\alpha} (\hat{c}_j^\dagger \hat{c}_{j-r} - \hat{c}_{j-r}^\dagger \hat{c}_j),$$

$$\hat{J}_{j,\text{out}} = -i \sum_r \frac{J}{r^\alpha} (\hat{c}_{j+r}^\dagger \hat{c}_j - \hat{c}_j^\dagger \hat{c}_{j+r}).$$ (3)

Our approach is based on analyzing the single particle correlation matrix $\mathbb{C}$ with matrix elements $C_{n,m}(t) = \text{Tr}[\rho(t)\hat{c}_n \hat{c}_m^\dagger]$, which for the noninteracting systems can be computed more efficiently [29,68–70]. The equation of motion for the correlation matrix is given by

$$\frac{\partial \mathbb{C}}{\partial t} = -i[\mathbb{H}, \mathbb{C}] - \{\mathbb{D}, \mathbb{C}\} + \mathbb{P},$$ (4)

where $(\mathbb{D})_{m,k} = \frac{\delta_{m,k}}{2}(\gamma + \Gamma[\delta_{m,1} + \delta_{m,N}])$, and $(\mathbb{P})_{m,k} = \delta_{m,k}[\gamma C_{m,m}(t) + \Gamma\delta_{m,N}\delta_{k,N}]$.

The NESS density profile and the current can be obtained from the elements of the correlation matrix $[C_{n,m}(t \to \infty)]$ as

$$\langle \hat{n}_m(\infty) \rangle = 1 - C_{m,m}(\infty),$$ (5)

$$J_\infty = \langle \hat{J}_m(\infty) \rangle = \sum_r \frac{2J}{r^\alpha} \text{Im}[C_{m,m-r}(\infty)].$$ (6)

In what follows, we will use current and resistance ($R_\infty = J_\infty^{-1}$) interchangeably in analyzing NESS transport and show our numerical findings. We focus on the NESS density profile throughout the lattice chain and the transport current from
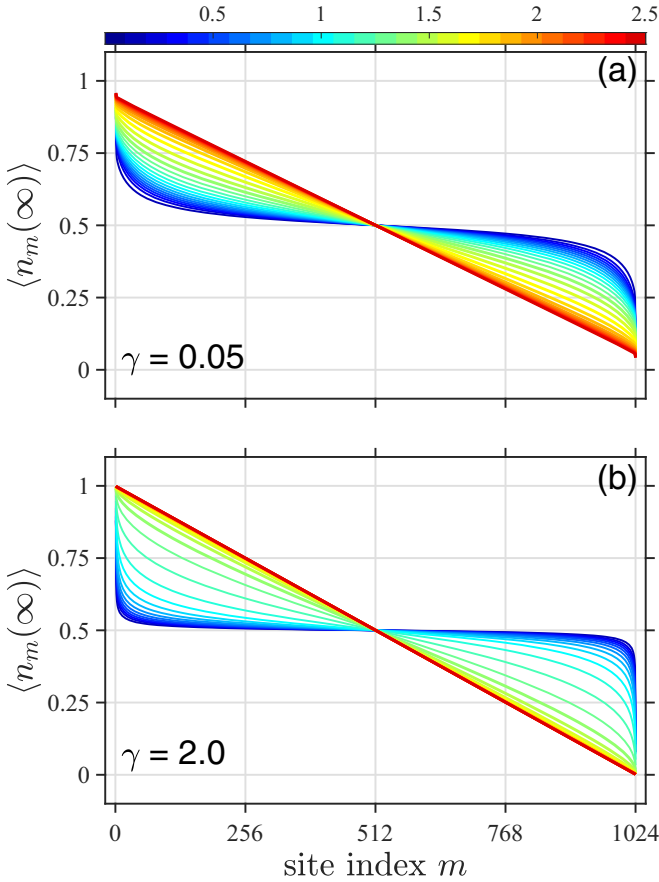
FIG. 2. Nonequilibrium steady-state density profile, viz., $\langle \hat{n}_m(\infty) \rangle$ with respect to the lattice site index, and for a range of long-range hopping parameter α. Upper (a) and lower (b) panels correspond to two different dephasing strengths $\gamma = 0.05$ and 2.0, respectively.

the right lead, viz., $J_\infty = \Gamma \langle \hat{n}_L(\infty) \rangle$. We study the system size scaling of the NESS current to characterize the various transport regimes. We fix the hopping amplitude $J = 1$. The dephasing strength γ and particle injection-extraction rate Γ are taken in the unit of J. In all the following analysis, we consider the system-lead coupling to be $\Gamma = 1$. It is a rather benign parameter compared to γ and α within our infinite bias setup as it only determines the overall magnitude of the current.

III. NESS DENSITY PROFILE AND CURRENT

We first study the steady-state density profile of the system and plot $\langle \hat{n}_m(\infty) \rangle$ as a function of the site index m for a range of long-range parameter α (shown in the color bar) in Fig. 2. We consider the dephasing strengths $\gamma = 0.05$ [upper panel in Fig. 2(a)] and $\gamma = 2.0$ [lower panel in Fig. 2(b)]. For $\alpha \neq 0$, and small dephasing strength $\gamma = 0.05$, the density profile shows a trend towards a linear profile for larger α values starting from a nonlinear profile at smaller α values. Although $\langle \hat{n}_m(\infty) \rangle$ shows the same trend towards a linear profile for larger dephasing, e.g., $\gamma = 2.0$ in Fig. 2, interestingly, $\langle \hat{n}_m(\infty) \rangle$ is more flattened in the bulk of the chain compared to the level of flatness seen for $\gamma = 0.05$. This is
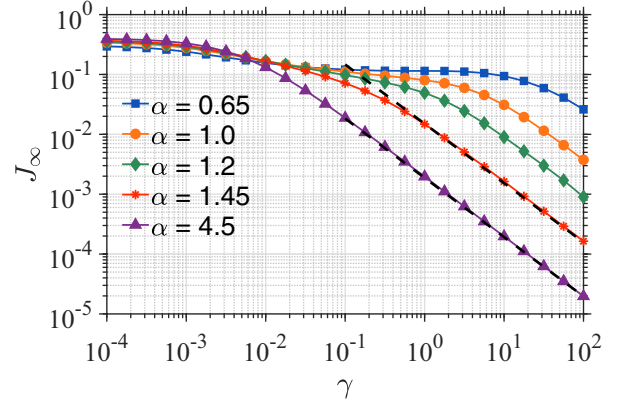
FIG. 3. Nonequilibrium steady-state current J_∞ corresponding to several values of α as a function of dephasing strength γ for system size $L = 1024$, in log-log scale. Black dashed lines correspond to $J_\infty \approx \frac{1}{\gamma}$ scaling.

opposite to the expectation; i.e., in the absence of dephasing, a chain with nearest-neighbor hopping exhibits a flat density profile in bulk with $\langle n_m(\infty) \rangle \approx 0.5$, a hallmark of ballistic transport, and, for stronger dephasing strength, the density profile scales as $\langle n_m(\infty) \rangle \propto 1/L$, suggesting a suppression in transport (diffusive transport). Such contrasting features hint towards the emergence of an interesting anomalous transport regime in the presence of long-range hopping.

To explore the regime of unusual transport, we study the variation of the NESS current J_∞ for different values of dephasing γ and long-range parameter α for a fixed system size $L = 1024$. Figure 3 plots J_∞ as a function of dephasing strength γ. We observe that the current gets suppressed with increased dephasing for all the values of α. This is clearly seen in Fig. 3 (black dashed lines) for $\alpha = 1.5$ and higher, where current decreases monotonically with γ, i.e., $J_\infty \propto \frac{1}{\gamma}$. For the short-range hopping model, in the absence of dephasing, the transport is always ballistic. Finite dephasing is detrimental to this ballistic transport and plays a role in inelastic scattering [29]. On the other side, for $\alpha < 1$, current initially decreases with increasing dephasing and, interestingly, settles down to a plateau regime for a considerable range $10^{-2} \lesssim \gamma \lesssim 10^1$ of dephasing. With increasing α, the range of γ over which this interesting plateau regime appears starts to shrink and eventually disappears for $\alpha \geqslant 1.5$. The plateau regime emerges due to the intricate interplay of long-range hopping and dephasing. In other words, due to long-range hopping, particles can now evade the inelastic scattering induced by the dephasing more easily and, thereby, can possibly deviate from standard diffusive transport.

In the following, we elaborate further on the appearance of the plateau and restrict ourselves to the dephasing strength $0.1 < \gamma < 2.0$, for which the J_∞ plateaus in Fig. 3. We plot a heat map of the J_∞ as a function of long-range parameter α and dephasing γ in Fig. 4, for $L = 1024$. We find that apart from the magnitude of J_∞, other features do not distinctively differ for different system sizes (see Supplemental Material [71]). First, we observe that NESS current becomes almost negligible for very small values of $\alpha \to 0$. In this limit, the system manifests all-to-all coupling that hinders transport and
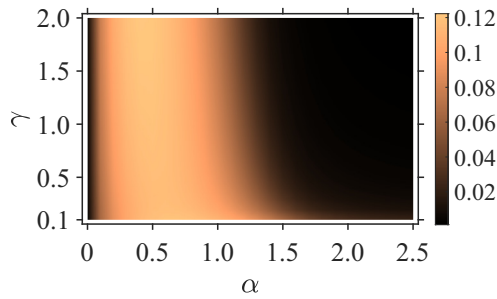
FIG. 4. The heat map of current $J_\infty = \langle \hat{J}_{L,\text{out}} \rangle$ as a function of the dephasing strength γ and long-range hopping exponent α. The color bar represents the magnitude of J_∞ for $L = 1024$.

incites cooperative shielding, akin to Anderson localization [72]. Intriguingly, this cooperative shielding is robust against the dephasing and system size L, as evident from Fig. 4. Then, for a finite α, we note a surge in NESS current, peaking near $\alpha \approx 0.6$ for values of $\gamma > 0.1$ and remaining almost independent of γ. Recall that this is reminiscent of the plateau observed in Fig. 3 for larger γ values for $\alpha = 0.65$. On further increasing the value of α, the plateau regime shrinks and eventually disappears for $\alpha > 1.5$ irrespective of γ, as seen from Fig. 4.

IV. NATURE OF THE NESS TRANSPORT

To understand the nature of the underlying NESS transport, we examine the system size scaling of the NESS resistance, denoted as $R_\infty = 1/J_\infty$, for various values of α. Note that the scaling results presented below are almost insensitive to γ for $\gamma > 0.1$. We, therefore, present results for $\gamma = 10$. Depending on the system size scaling of R_∞ different transport regimes are classified, namely, for ballistic transport $R_\infty \sim L^0$ [73] and for diffusive or normal transport $R_\infty \sim L$ [29]. Anything away from these scaling relations is often categorized as anomalous transport, for example, $R_\infty \sim L^\nu$ with $\nu > 1$ is subdiffusive [56] whereas for $\nu < 1$ it is superdiffusive.

In Fig. 5, we demonstrate the system size scaling of R_∞ for different values of α to analyze the regimes of transport.
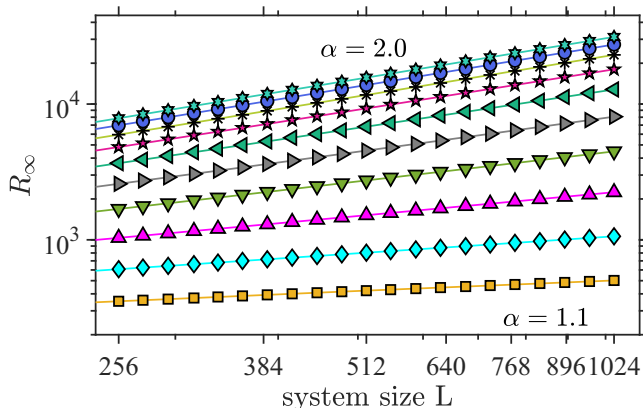
FIG. 5. NESS resistance $R_\infty = 1/J_\infty$ as a function of system size L on a log-log scale from $\alpha = 1.1$ to 2.0 (bottom to top) in an increment of 0.1.
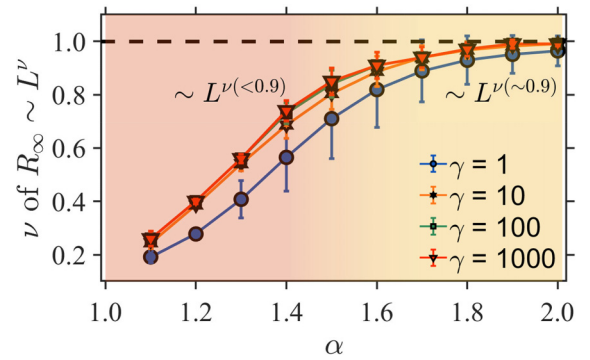
FIG. 6. Transport exponent ν obtained from the fit $R_\infty \sim L^\nu$ as a function of α for $\alpha > 1.0$ and different values of dephasing strength γ. The error bars are associated with the fitting of $R_\infty \sim L^\nu$.

In Fig. 5(a), we first concentrate on $\alpha \leqslant 1$. We plot R_∞ as a function of system size L for $\alpha = 0.9$ and 1.0. Interestingly, we observe logarithmic system size scaling, $R_\infty \sim \log(L)$, as clear from the straight-line fitting of the numerical data on a log-linear scale. This clearly demonstrates an anomalous superdiffusive transport regime for $\alpha \leqslant 1$. Next, in Fig. 5(b) we focus on the case of $\alpha > 1$. We plot R_∞ as a function of L for $1.0 < \alpha \leqslant 2$. Remarkably, in this regime of α we observe a power-law dependence: $R_\infty \sim L^\nu$ with an α-dependent exponent ν. This is evident from the plot of R_∞ on a log-log scale. Therefore, it is clear from Figs. 5(a) and 5(b) that as α increases beyond the value 1, the scaling of R_∞ changes from a logarithmic to a power-law behavior in system size.

To further elaborate on the nature of the transport for $\alpha > 1$, we plot the dependence of the transport exponent ν with α in Fig. 6. Our numerical calculations show that ν increases with increasing α before saturating beyond $\alpha \gtrsim 1.6$. In fact, we find from numerical calculations that $\nu \approx 2\alpha - 2$ for $\alpha \lesssim 1.6$. It is worth mentioning that the superdiffusive transport for $1.0 < \alpha \lesssim 1.6$ is extremely robust against the dephasing strength. However, a finite amount of dephasing along with the long-range hopping is necessary to observe the emergence of these intriguing transport regimes. Remarkably, for $\alpha \gtrsim 1.6$, a diffusive transport regime sets in independent of the value of dephasing. However, we show below that the transition from superdiffusive to diffusive transport in the thermodynamic limit happens exactly at $\alpha = 1.5$. We believe this difference is due to the finite-size effect.

To substantiate the above numerical observation that a diffusive transport emerges only for $\alpha > 1.5$, we show that the behavior of the current-operator norm (in the absence of the dephasing), analogously to the Hamiltonian operator norm discussed in [61], can provide more insightful information. We start by writing down the operator for current into the site L as

$$\hat{J}_{L,\text{in}} = -i \sum_{r=1}^{L-1} \frac{J}{r^\alpha} (\hat{c}_{L-r}^\dagger \hat{c}_L - \hat{c}_L^\dagger \hat{c}_{L-r}). \tag{7}$$

The corresponding operator norm $||J_L|| = \text{Tr}(\sqrt{\hat{J}_L^\dagger \hat{J}_L})$ exhibits the following system-size dependence (see [71] for the details

of calculation):

$$||J_L|| \sim \frac{L^{3/2-\alpha}}{\sqrt{(2\alpha-1)(3/2-\alpha)}}, \text{ for } \alpha < 1.5,$$

$$\sim \text{constant independent of } L \text{ for } \alpha > 1.5. \quad (8)$$

The current-operator norm, which indicates the maximum possible coherent particle transport rate, does not change with L when $\alpha > 1.5$. Therefore, in a finite-size system, sufficiently high dephasing strength can hinder coherent transport, causing diffusive transport. In fact, for $\alpha > 1.5$, it suggests that any finite dephasing can prompt a diffusive transport in the thermodynamic limit, akin to what is seen in short-range systems [74].

For $\alpha < 1.5$, the current-operator norm diverges with system size, implying that no amount of dephasing is enough to cause diffusive or subdiffusive transport in the thermodynamic limit. Furthermore, the presence of an extensive number of dephasing sites along with the scaling of the current norm suggests the absence of a ballistic transport, leaving the possibility of superdiffusive transport. Thus, the operator norm scaling in the absence of the dephasing highlights $\alpha = 1.5$ as a critical point, helping explain the crossover from superdiffusive to diffusive transport in the presence of dephasing.

V. SUMMARY AND DISCUSSION

In summary, due to a nontrivial interplay between the long-range hopping and the dephasing strength, we have found the emergence of distinctive regimes of NESS transport as one tunes the long-range exponent α. Specifically, we demonstrate that for $\alpha > 1.5$ the transport is diffusive/normal, whereas, for $\alpha < 1.5$, the transport is superdiffusive. Furthermore, we observe two different system-size scalings within the superdiffusive regime; namely, for $1 < \alpha < 1.5$, we find a power-law system size dependence with an α-dependent exponent $\nu < 1$, and for $\alpha \leqslant 1$ we observe inverse-logarithmic system size scaling for the current. Remarkably, the superdiffusive regime is robust against the dephasing strength. We further provide analytical insights to support our numerical findings by analyzing the current-operator norm.

It is worth pointing out that the heat map of the NESS current on the α-γ plane, as presented in Fig. 4, bears a close resemblance to the phase diagram of entanglement measures related to the MIPT [61]. Unlike our steady-state solution of the Lindblad quantum master equation, the transition of entanglement entropy from an area law phase to a volume law phase in MIPT emerges through a specific unraveling of the Lindblad master equation. For free fermions in one dimension

(without the boundary drive), MIPT appears at the long-range exponent $\alpha = 1.5$ [61]. Intriguingly, in our setup, a transition from superdiffusive to diffusive regime also appears at the same long-range exponent value, i.e., $\alpha = 1.5$. Given that number-conserving local dephasing in our setup acts like a Zeno-type local number density measurement, our results hint at a possible connection between the MIPT and the transition from anomalous to normal transport observed in the NESS current.

However, our identification of transport as a possible signature of the underlying MIPT is not caveat free. Indeed, the absence of a direct link between mutual information and particle current renders such an identification nontrivial, positing an intriguing avenue for future research. Relevantly, prior numerical analyses have pointed out interesting connections between NESS transport current and entanglement measures, like mutual information and concurrence, particularly in quantum dot setups [75–77]. Establishing a more rigorous link could pave the way for discerning MIPT in experiments via current measurements. Additionally, when the boundary drive is absent, our setup can be considered a long-range hopping system subjected to time-dependent delta-correlated classical Gaussian noise, where the particle density profile follows a fractional diffusion equation [78,79]. However, an intriguing question for future exploration is how the presence of the boundary drive, akin to quantum noise, alters this diffusion-like equation.

[1] E. Z. Harush and Y. Dubi, Do photosynthetic complexes use quantum coherence to increase their efficiency? Probably not, Sci. Adv. **7**, eabc4631 (2021).

[2] A. Mattioni, F. Caycedo-Soler, S. F. Huelga, and M. B. Plenio, Design principles for long-range energy transfer at room temperature, Phys. Rev. X **11**, 041003 (2021).

[3] C. Maier, T. Brydges, P. Jurcevic, N. Trautmann, C. Hempel, B. P. Lanyon, P. Hauke, R. Blatt, and C. F. Roos, Environment-assisted quantum transport in a 10-qubit network, Phys. Rev. Lett. **122**, 050501 (2019).

[4] P. Barthelemy and L. M. K. Vandersypen, Quantum dot systems: A versatile platform for quantum simulations, Ann. Phys. (Leipzig) **525**, 808 (2013).

[5] S. Sarkar and Y. Dubi, Emergence and dynamical stability of a charge time-crystal in a current-carrying quantum dot simulator, Nano Lett. **22**, 4445 (2022).

[6] S. Sarkar and Y. Dubi, Signatures of discrete time-crystallinity in transport through an open fermionic chain, Commun. Phys. **5**, 155 (2022).

[7] M. Field, C. G. Smith, M. Pepper, D. A. Ritchie, J. E. F. Frost, G. A. C. Jones, and D. G. Hasko, Measurements of Coulomb blockade with a noninvasive voltage probe, Phys. Rev. Lett. **70**, 1311 (1993).

[8] T. Byrnes, N. Y. Kim, K. Kusudo, and Y. Yamamoto, Quantum simulation of Fermi-Hubbard models in semiconductor quantum-dot arrays, Phys. Rev. B **78**, 075320 (2008).

[9] V. V. Deshpande, M. Bockrath, L. I. Glazman, and A. Yacoby, Electron liquids and solids in one dimension, Nature (London) **464**, 209 (2010).

[10] D. Loss and D. P. DiVincenzo, Quantum computation with quantum dots, Phys. Rev. A **57**, 120 (1998).

[11] R. Steinigeweg, H. Wichterich, and J. Gemmer, Density dynamics from current auto-correlations at finite time- and length-scales, Europhys. Lett. **88**, 10004 (2009).

[12] Y. Bar Lev, G. Cohen, and D. R. Reichman, Absence of diffusion in an interacting system of spinless fermions on a one-dimensional disordered lattice, Phys. Rev. Lett. **114**, 100601 (2015).

[13] R. Steinigeweg, F. Jin, D. Schmidtke, H. De Raedt, K. Michielsen, and J. Gemmer, Real-time broadening of nonequilibrium density profiles and the role of the specific initial-state realization, Phys. Rev. B **95**, 035155 (2017).

[14] D. J. Luitz and Y. B. Lev, The ergodic side of the many-body localization transition, Ann. Phys. (Leipzig) **529**, 1600350 (2017).

[15] M. Žnidarič, Dephasing-induced diffusive transport in the anisotropic Heisenberg model, New J. Phys. **12**, 043001 (2010).

[16] M. Žnidarič and M. Horvat, Transport in a disordered tight-binding chain with dephasing, Eur. Phys. J. B **86**, 67 (2013).

[17] M. Žnidarič, J. J. Mendoza-Arenas, S. R. Clark, and J. Goold, Dephasing enhanced spin transport in the ergodic phase of a many-body localizable system, Ann. Phys. (Leipzig) **529**, 1600298 (2017).

[18] B. Bertini, F. Heidrich-Meisner, C. Karrasch, T. Prosen, R. Steinigeweg, and M. Žnidarič, Finite-temperature transport in one-dimensional quantum lattice models, Rev. Mod. Phys. **93**, 025003 (2021).

[19] V. Eisler, Crossover between ballistic and diffusive transport: the quantum exclusion process, J. Stat. Mech.: Theory Exp. (2011) P06007.

[20] M. Esposito and P. Gaspard, Emergence of diffusion in finite quantum systems, Phys. Rev. B **71**, 214302 (2005).

[21] M. Esposito and P. Gaspard, Exactly solvable model of quantum diffusion, J. Stat. Phys. **121**, 463 (2005).

[22] T. L. M. Lezama and Y. Bar Lev, Logarithmic, noise-induced dynamics in the Anderson insulator, SciPost Phys. **12**, 174 (2022).

[23] D. S. Bhakuni, T. L. Lezama, and Y. B. Lev, Noise-induced transport in the Aubry-André-Harper model, arXiv:2307.06373.

[24] B. Gu and I. Franco, When can quantum decoherence be mimicked by classical noise? J. Chem. Phys. **151**, 014109 (2019).

[25] E. Zerah-Harush and Y. Dubi, Effects of disorder and interactions in environment assisted quantum transport, Phys. Rev. Res. **2**, 023294 (2020).

[26] P. Rebentrost, M. Mohseni, I. Kassal, S. Lloyd, and A. Aspuru-Guzik, Environment-assisted quantum transport, New J. Phys. **11**, 033003 (2009).

[27] S. Sarkar and Y. Dubi, Environment-assisted and environment-hampered efficiency at maximum power in a molecular photocell, J. Phys. Chem. C **124**, 15115 (2020).

[28] S. Gopalakrishnan, K. R. Islam, and M. Knap, Noise-induced subdiffusion in strongly localized quantum systems, Phys. Rev. Lett. **119**, 046601 (2017).

[29] X. Turkeshi and M. Schiró, Diffusion and thermalization in a boundary-driven dephasing model, Phys. Rev. B **104**, 144301 (2021).

[30] M. Saha, B. P. Venkatesh, and B. K. Agarwalla, Quantum transport in quasiperiodic lattice systems in the presence of Büttiker probes, Phys. Rev. B **105**, 224204 (2022).

[31] P. Richerme, Z.-X. Gong, A. Lee, C. Senko, J. Smith, M. Foss-Feig, S. Michalakis, A. V. Gorshkov, and C. Monroe, Non-local propagation of correlations in quantum systems with long-range interactions, Nature (London) **511**, 198 (2014).

[32] P. Jurcevic, B. P. Lanyon, P. Hauke, C. Hempel, P. Zoller, R. Blatt, and C. F. Roos, Quasiparticle engineering and entanglement propagation in a quantum many-body system, Nature (London) **511**, 202 (2014).

[33] M. Gring, M. Kuhnert, T. Langen, T. Kitagawa, B. Rauer, M. Schreitl, I. Mazets, D. Adu Smith, E. Demler, and J. Schmiedmayer, Relaxation and prethermalization in an isolated quantum system, Science **337**, 1318 (2012).

[34] W. Morong, F. Liu, P. Becker, K. S. Collins, L. Feng, A. Kyprianidis, G. Pagano, T. You, A. V. Gorshkov, and C. Monroe, Observation of Stark many-body localization without disorder, Nature (London) **599**, 393 (2021).

[35] A. Kyprianidis, F. Machado, W. Morong, P. Becker, K. S. Collins, D. V. Else, L. Feng, P. W. Hess, C. Nayak, G. Pagano, N. Y. Yao, and C. Monroe, Observation of a prethermal discrete time crystal, Science **372**, 1192 (2021).

[36] J. M. Kosterlitz, Phase transitions in long-range ferromagnetic chains, Phys. Rev. Lett. **37**, 1577 (1976).

[37] T. Kuwahara and K. Saito, Area law of noncritical ground states in 1D long-range interacting systems, Nat. Commun. **11**, 4478 (2020).

[38] T. Koffel, M. Lewenstein, and L. Tagliacozzo, Entanglement entropy for the long-range ising chain in a transverse field, Phys. Rev. Lett. **109**, 267203 (2012).

[39] D. Vodola, L. Lepori, E. Ercolessi, A. V. Gorshkov, and G. Pupillo, Kitaev chains with long-range pairing, Phys. Rev. Lett. **113**, 156402 (2014).

[40] D. Vodola, L. Lepori, E. Ercolessi, and G. Pupillo, Long-range Ising and Kitaev models: Phases, correlations and edge modes, New J. Phys. **18**, 015001 (2015).

[41] C.-F. Chen and A. Lucas, Finite speed of quantum scrambling with long range interactions, Phys. Rev. Lett. **123**, 250605 (2019).

[42] M. C. Tran, C.-F. Chen, A. Ehrenberg, A. Y. Guo, A. Deshpande, Y. Hong, Z.-X. Gong, A. V. Gorshkov, and A. Lucas, Hierarchy of linear light cones with long-range interactions, Phys. Rev. X **10**, 031009 (2020).

[43] T. Kuwahara and K. Saito, Strictly linear light cones in long-range interacting systems of arbitrary dimensions, Phys. Rev. X **10**, 031010 (2020).

[44] T. Zhou, S. Xu, X. Chen, A. Guo, and B. Swingle, Operator Lévy flight: Light cones in chaotic long-range interacting systems, Phys. Rev. Lett. **124**, 180601 (2020).

[45] T. Kuwahara and K. Saito, Absence of fast scrambling in thermodynamically stable long-range interacting systems, Phys. Rev. Lett. **126**, 030604 (2021).

[46] R. M. Nandkishore and S. L. Sondhi, Many-body localization with long-range interactions, Phys. Rev. X **7**, 041021 (2017).

[47] M. F. Maghrebi, Z.-X. Gong, and A. V. Gorshkov, Continuous symmetry breaking in 1D long-range interacting quantum systems, Phys. Rev. Lett. **119**, 023001 (2017).

[48] J. Schachenmayer, B. P. Lanyon, C. F. Roos, and A. J. Daley, Entanglement growth in quench dynamics with variable range interactions, Phys. Rev. X **3**, 031015 (2013).

[49] A. Lerose and S. Pappalardi, Origin of the slow growth of entanglement entropy in long-range interacting spin systems, Phys. Rev. Res. **2**, 012041(R) (2020).

[50] D. S. Bhakuni, L. F. Santos, and Y. B. Lev, Suppression of heating by long-range interactions in periodically driven spin chains, Phys. Rev. B **104**, L140301 (2021).

[51] L. F. Santos, F. Borgonovi, and G. L. Celardo, Cooperative shielding in many-body systems with long-range interaction, Phys. Rev. Lett. **116**, 250402 (2016).

[52] D. M. Storch, M. Van Den Worm, and M. Kastner, Interplay of soundcone and supersonic propagation in lattice models with power law interactions, New J. Phys. **17**, 063021 (2015).

[53] H. N. Nazareno and P. E. de Brito, Long-range interactions and nonextensivity in one-dimensional systems, Phys. Rev. B **60**, 4629 (1999).

[54] G. Lindblad, On the generators of quantum dynamical semigroups, Commun. Math. Phys. **48**, 119 (1976).

[55] V. Gorini, A. Kossakowski, and E. C. G. Sudarshan, Completely positive dynamical semigroups of n-level systems, J. Math. Phys. **17**, 821 (1976).

[56] A. Purkayastha, M. Saha, and B. K. Agarwalla, Subdiffusive phases in open clean long-range systems, Phys. Rev. Lett. **127**, 240601 (2021).

[57] G. Wójtowicz, J. E. Elenewski, M. M. Rams, and M. Zwolak, Open-system tensor networks and Kramers' crossover for quantum transport, Phys. Rev. A **101**, 050301(R) (2020).

[58] G. Wójtowicz, A. Purkayastha, M. Zwolak, and M. M. Rams, Accumulative reservoir construction: Bridging continuously relaxed and periodically refreshed extended reservoirs, Phys. Rev. B **107**, 035150 (2023).

[59] M. Block, Y. Bao, S. Choi, E. Altman, and N. Y. Yao, Measurement-induced transition in long-range interacting quantum circuits, Phys. Rev. Lett. **128**, 010604 (2022).

[60] T. Müller, S. Diehl, and M. Buchhold, Measurement-induced dark state phase transitions in long-ranged fermion systems, Phys. Rev. Lett. **128**, 010605 (2022).

[61] T. Minato, K. Sugimoto, T. Kuwahara, and K. Saito, Fate of measurement-induced phase transition in long-range interactions, Phys. Rev. Lett. **128**, 010603 (2022).

[62] N. Defenu, Metastability and discrete spectrum of long-range systems, Proc. Natl. Acad. Sci. USA **118**, e2101785118 (2021).

[63] M. Kastner, Diverging equilibration times in long-range quantum spin models, Phys. Rev. Lett. **106**, 130601 (2011).

[64] M. Kastner, N-scaling of timescales in long-range N-body quantum systems, J. Stat. Mech.: Theory Exp. (2017) 014003.

[65] R. Bachelard and M. Kastner, Universal threshold for the dynamical behavior of lattice systems with long-range interactions, Phys. Rev. Lett. **110**, 170603 (2013).

[66] T. Jin, J. a. S. Ferreira, M. Filippone, and T. Giamarchi, Exact description of quantum stochastic models as quantum resistors, Phys. Rev. Res. **4**, 013109 (2022).

[67] B. Neyenhuis, J. Zhang, P. W. Hess, J. Smith, A. C. Lee, P. Richerme, Z. X. Gong, A. V. Gorshkov, and C. Monroe, Observation of prethermalization in long-range interacting spin chains, Sci. Adv. **3**, e1700672 (2017).

[68] J. E. Elenewski, D. Gruss, and M. Zwolak, Communication: Master equations for electron transport: The limits of the Markovian limit, J. Chem. Phys. **147**, 151101 (2017).

[69] M. Zwolak, Analytic expressions for the steady-state current with finite extended reservoirs, J. Chem. Phys. **153**, 224107 (2020).

[70] V. K. Varma, C. de Mulatier, and M. Žnidarič, Fractality in nonequilibrium steady states of quasiperiodic systems, Phys. Rev. E **96**, 032130 (2017).

[71] See Supplemental Material at http://link.aps.org/supplemental/10.1103/PhysRevB.109.165408 for (I) System size dependence of heat map for NESS current and (II) Operator norm scaling of current and proof for Eq. (8).

[72] G. L. Celardo, R. Kaiser, and F. Borgonovi, Shielding and localization in the presence of long-range hopping, Phys. Rev. B **94**, 144206 (2016).

[73] A. Dhar and D. Roy, Heat transport in harmonic lattices, J. Stat. Phys. **125**, 801 (2006).

[74] M. Žnidarič, Exact solution for a diffusive nonequilibrium steady state of an open quantum chain, J. Stat. Mech.: Theory Exp. (2010) L05002.

[75] A. Sharma and E. Rabani, Landauer current and mutual information, Phys. Rev. B **91**, 085121 (2015).

[76] H. S. Sable, D. S. Bhakuni, and A. Sharma, Landauer current and mutual information in a bosonic quantum dot, J. Phys.: Conf. Ser. **964**, 012007 (2018).

[77] A. Dey, D. S. Bhakuni, B. K. Agarwalla, and A. Sharma, Quantum entanglement and transport in a non-equilibrium interacting double-dot system: The curious role of degeneracy, J. Phys.: Condens. Matter **32**, 075603 (2020).

[78] M. K. Joshi, F. Kranzl, A. Schuckert, I. Lovas, C. Maier, R. Blatt, M. Knap, and C. F. Roos, Observing emergent hydrodynamics in a long-range quantum magnet, Science **376**, 720 (2022).

[79] A. Schuckert, I. Lovas, and M. Knap, Nonlocal emergent hydrodynamics in a long-range quantum spin system, Phys. Rev. B **101**, 020416(R) (2020).